

Legends to Extended Data Figures

Extended Data Figure 1. Schematic model of the interplay between autophagy and ciliogenesis. Starvation conditions (serum-) increase intraflagellar transport (IFT) and ciliogenesis and Hedgehog (Hh) signaling. We show in this work that both events increase autophagosome formation interdependently. Atg16L is trafficked in IFT20- enriched vesicles to the base of the cilia where most Atg localize. Arrival of Atg16L to this Atg assembly and/or its transport along the axoneme seems to initiate the elongation of Atg5 structures and presence of lipid-binding Atgs (such as LC3 and GABARAP) in the cilia and at the plasma membrane. The cilium also contains under these conditions molecules of Smo that are mobilized to the ciliary membrane after release of the inhibitory effect of Ptc. Activated Smo induces the downstream transcription factors Gli1/2 which further favors recruitment and assembly of Atgs in the base of the cilium. Normal nutritional conditions (serum+) lead to decreased Hh and IFT and suppression of starvation-induced autophagy. Basal autophagy contributes to maintain ciliogenesis to a minimum through the degradation of IFT20, which in turns reduces trafficking of Atg16L into the Atg assembly at the base of the cilium, preventing induction of ciliary autophagy.

Extended Data Figure 2. Ciliogenesis and LC3 in different cell types. (a) Immunoblot for IFT20 and IFT88 and quantification in MEFs control (Ctrl) or knocked down (-) for IFT20 (**p=0.007, n=7), or kidney epithelial cells (KECs) wild-type (wt) or knock-out for IFT88 (IFT88^{-/-}; **p=0.0003, n=3). ADU: arbitrary densitometric units (n=3). (b) Rates of degradation of long-lived proteins in the same cells expressed as percentage of total proteolysis (top) or as percentage of lysosomal degradation (sensitive to inhibition of lysosomal proteases) (*p=0.021, n=3). (c) Ciliated cells in MEFs (**p=0.003, n=5), KECs (*p=0.011, *p=0.021, n=5) and retinal ganglion cells (RGC-5; **p=0.004, ##p=0.0002, n=5) maintained in the presence or absence of serum. (d) Immunoblot for LC3 in MEFs and KECs maintained in the presence of serum and treated or not with protease inhibitors (PI). (e) Single channel images and merge of wt and IFT88^{-/-} KECs transfected with the mCherry-GFP-LC3 reporter. (f) Immunofluorescence for LC3 in wt and IFT88^{-/-} KECs upon serum removal. Quantification of LC3-positive puncta (*p=0.04, n=3). Bars: 10µm. Mean±s.e.m unless otherwise stated.

Extended Data Figure 3. Autophagy in IFT88 and IFT20 double knock-down cells. (a) Immunoblot for the indicated proteins of MEFs Ctrl or knock-down for IFT88 (IFT88(-)) or for IFT88 and IFT20 (IFT20(-)/IFT88(-)). (b) Percentage of ciliated cells after 24h serum starvation and representative images of cilia (acetylated tubulin, green) and basal body (γ-tubulin, red) in the same cells (IFT88(-), **p=0.00001; IFT20-88(-), **p=0.0006, n=5). Arrows indicate cilia. (c) LC3 flux immunoblot in the same cell lines maintained in presence or absence of serum. (d) Quantification of LC3-II levels (S+, **p=0.0008, **p=0.004, n=4; S-, *p=0.034, n=5) and LC3-II flux (S+, n=4; S-, *p=0.016, n=5) by densitometry of blots as the ones shown in c. Mean±s.d. (e) LC3 flux in a retinal ganglion cell line (RGC-5) and in KEC treated or not with platelet-derived growth factor (PDGF). Bars: 10µm. Mean±s.e.m unless otherwise stated.

Extended Data Figure 4. Ciliary hedgehog signaling modulates autophagy. (a) Scheme of chemical and genetic approaches to modulate hedgehog (Hh) signaling. Both the agonist purmorphamine (Purmo) and genetic ablation of the Patched-1 receptor (Ptc^{-/-}) result in the recruitment of Smo to the cilia and initiation of expression of Gli factors. Knock-down of Smo(-) or treatment with the Smo antagonist cyclopamine (Cyclo) suppress activation of downstream effectors. (b) mRNA expression of Hh downstream effector genes relative after PDGF-induced ciliary resorption relative to untreated Serum- cells (Gli1, **p=0.0006, **p=0.007; Gli2, **p=0.0001; Ptc, **p=0.002; n=3). (c) mRNA levels for downstream target genes of Hh signaling measured by RT-PCR after the indicated treatments (Smo; Ctrl *p=0.028, purmo *p=0.027; Gli1,

ctrl **p=0.006, Purmo *p=0.037; Bcl-2, Ctrl **p=0.007; n=3). **(d)** Immunofluorescence for LC3 in control cells treated or not with Purmo, and in Ptc^{-/-} cells. Right: quantification (n=3). **(e)** mCherry-GFP-LC3 reporter in cells treated with Purmo. **(f)** LC3 flux in IFT88(-) MEFs treated with Purmo. Right: Quantification of LC3-II flux (Mean±s.d.;n=3). **(g)** Ptc mRNA levels in MEF wt and Ptc1^{-/-} (n=3). **(h)** Immunofluorescence for acetylated tubulin in MEF wt and Ptc^{-/-}. **(i)** Percentage ciliated cells in wt and Ptc^{-/-} MEFs (*p0.014, ###p=0.0009, n=3). **(j)** Relative mRNA expression by RT-PCR of Hh downstream effector genes in control and myc-Gli1 cells (Gli1, **p=0.0017; Bcl2 **p=0.004; Ptc **p=0.0006; Hhip *p=0.03; Gli2 *p=0.028; n=3). **(k)** LC3 flux immunoblot in MEFs treated or not with Cyclo, and PI. Quantification of LC3-II flux (n=3). Differences with Ctrl (*) or with Serum + (#) are significant for p<0.05. n.s., statistically non-significant. Mean±s.e.m unless otherwise stated. Bars: 10µm.

Extended Data Figure 5. Presence of Atgs at the primary cilia. **(a)** Co-immunostaining for the indicated autophagy-related proteins (Atgs; green) and acetylated tubulin (red) of mouse kidney epithelial cells maintained in the absence of serum for 24h. **(b)** 3D reconstruction of the co-staining for Atg16L and acetylated tubulin in the cilia. Atg14 is shown as an example of absence of colocalization. 0.2 µm Z-stack are shown from the surface to the bottom part of the cilium. **(c)** Staining with Atg16L or acetylated tubulin, and 3D images in cells transiently transfected with either GFP-LC3 or GFP-inversin and in GFP-inversin 3T3 stable cell lines. **(d)** Immunostaining for Atg16L in NRK Ctr or knock-down for Atg16L transiently transfected with GFP-inversin to highlight the primary cilia. Individual channels, merge and 3D reconstitution of the co-staining are shown. **(e)** Immunoblot for Atg16L in Atg16L(-) NRK cells. Bars: 10µm.

Extended Data Figure 6. Autophagy-related proteins associate with the basal body in a serum-dependent manner. Co-immunostaining for Atgs and gamma tubulin of kidney epithelial cells (KECs) maintained in serum-free **(a)** or serum-supplemented media **(b)** Arrows: colocalization (yellow) or no colocalization (white) in the centriole. **(c)** Co-immunostaining of Atg7 (green) with gamma tubulin (red) in wt and IFT88^{-/-} KECs maintained in the presence or absence of serum for 24h. Bars: 10µm.

Extended Data Figure 7. Changes in intracellular distribution of Atgs in kidney epithelial cells with defective IFT. **(a)** Immunostaining for Atg7, Atg14, LC3 and GABARAP in wt and IFT88^{-/-} kidney epithelial cells (KECs) maintained in the presence or absence of serum for 24h. **(b)** Atg5 co-immunostaining (green) with gamma tubulin or acetylated tubulin (red) in KECs. Arrows indicate clusters of Atg5. **(c)** Immunostaining for Atg5 in wt and IFT88^{-/-} KECs maintained in the absence of serum for 24h. **(d)** Immunostaining for Atg5 (green) and acetylated tubulin (red) in wt or Ptc^{-/-} MEFs. Yellow arrow: Atg5 over ciliary structures. Bars: 10µm.

Extended Data Figure 8. Interaction of IFT20 with Atgs. **(a)** Co-immunostaining for Atg16L and γ-tubulin in kidney epithelial cells (KECs) wt or IFT88^{-/-} maintained in the presence or absence of serum for 24h. Arrows: colocalization (yellow) or no colocalization (white) at the basal body (BB). **(b)** Percentage of wt MEFs untreated (-), treated with Purmo (*p=0.01, n=4) or Ptc^{-/-} (*p=0.005, n=4) showing colocalization of Atg16L and BB in the absence of serum. **(c)** Co-immunostaining for IFT20 and Atg16L in the same cells as in **a**. Insets show split channels of boxed areas at higher magnification. Arrows: colocalization. Right: Quantification of the colocalization (###p=0.004, **p=0.004, n=4). **(d)** Co-immunostaining for IFT20 (red) with Vps15, Atg7 and Atg14 (green) in wt KECs during starvation. Insets show boxed areas at higher magnification. Yellow arrows: colocalization. Percentage of colocalization is indicated. **(e-g)** Immunoblot for the indicated proteins after coimmunoprecipitation for IFT20 **(e,f)** or Atg14 **(g)** in the same cells. **(h)** Immunogold electron microscopy for Atg16L and IFT20 in isolated cytosolic vesicles. Full field images of double immunogold staining for IFT20 (10nm) and Atg16L (15nm)

captured by transmission electron microscopy. Atg16L alone (yellow), IFT20 alone (blue) both proteins (red). Right image shows absence of gold particles in a region of vesicle-free film. Mean \pm s.e.m unless otherwise stated. Bars: 10 μ m.

Extended Data Figure 9. Effect of blockage of autophagy on ciliogenesis. (a) Co-immunostaining for acetylated tubulin and gamma tubulin in MEFs from wild type (wt) or Atg5 null mice (Atg5^{-/-}) maintained in the absence of serum for the indicated periods of time. Arrows: cilia. (b) Immunostaining for acetylated and gamma tubulin in MEFs control or knocked-down (-) for Atg7, and maintained in the presence or absence of serum. Arrows: cilia. (c) Quantification of the percentage of ciliated cells in Atg7(-) (n=5). (d) Immunostaining for acetylated tubulin in KEC control or Atg14(-). (e) Quantification of the percentage of ciliated cells in Atg14(-) cells. Cells from IFT88 null mice are used as negative control in e. (n=4). (f) Percentage of ciliated MEFs upon treatment with 3-methyladenine (3MA) or rapamycin (Rapa) in the presence or absence of serum (n=3). (g) Percentage of ciliated retinal ganglionar cells (RGC-5) at the indicated times of treatment with 3MA or rapamycin in the presence of serum (n=3). Bars: 10 μ m. Arrows; cilia. All values are mean \pm s.e.m unless otherwise stated. Differences with Ctrl (*) or with Serum+ (#) are significant for p<0.05. n.s., statistically non-significant.

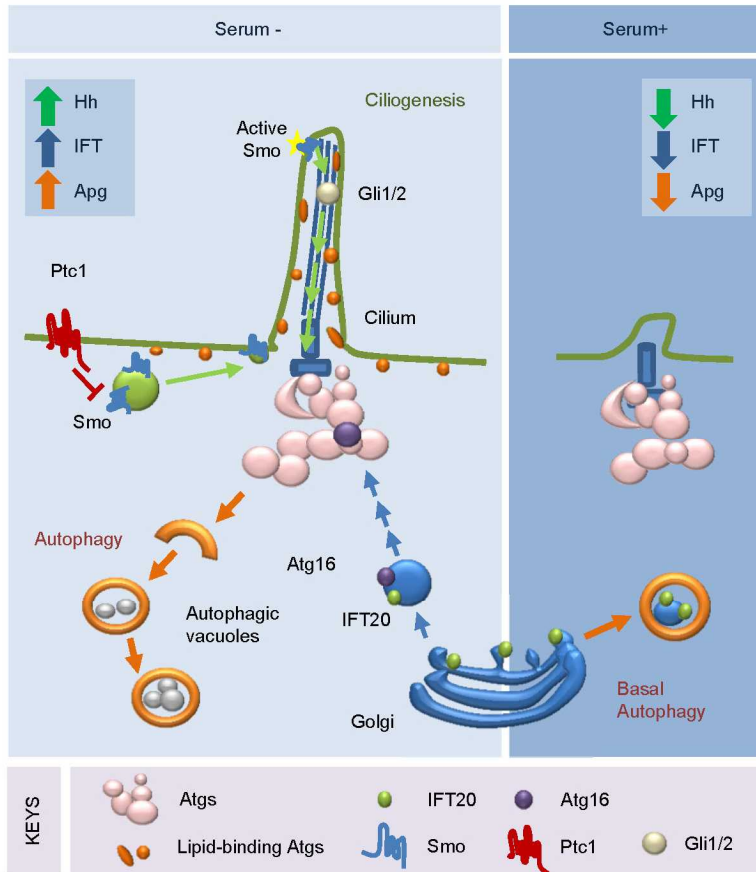
Extended Data Figure 10. Ultrastructure of the primary cilia in autophagy-deficient cells. Scanning electron microscopy images of embryonic fibroblasts from wild-type (wt) and Atg5-defective mice (-/-) grown in the absence or presence of serum. (a) Surface of the different cells to highlight lower levels of villi in the Atg5^{-/-} cells. Red arrow: primary cilia. (b) Details of primary cilia. Arrows: cilia-associated vesicles. Arrowhead: ciliary pocket. (c-e) Morphometric analysis of the cilia; cilia diameter (S- **p=0.0002, n=28; S+, **p=0.026, n=24) (c), area of the ciliary pocket (S-, **p=0.009, n=28; S+, **p=0.0001; n=24) (d), and exosome diameter and number of exosomes per cilia (e) in wt and Atg5^{-/-} MEFs. Mean \pm s.d.

Extended Data Figure 11. Enhanced ciliogenesis in autophagy deficient cells. (a) Co-immunostaining for Smo an acetylated tubulin in wt and Atg5^{-/-} MEFs treated or not with Purmo. Arrows: colocalization (yellow) or no colocalization (white). (b) Immunofluorescence for IFT20 in MEF wt and Atg5^{-/-}. Arrows; IFT20 cytosolic vesicles. Bars: 10 μ m. All values are mean \pm s.e.m unless otherwise stated. (c) Immunoblot for the indicated proteins in wt MEFs treated or not with ammonium chloride and leupeptin (N/L) and collected at different times after serum removal. (d) Time-course of changes in IFT20 protein levels in wt and Atg5^{-/-} cells during serum removal relative to levels in serum supplemented wt MEFs. Time-course of changes in LC3-II flux is plotted as discontinuous line.

Type of file: figure

Label: Extended Data Figure 1

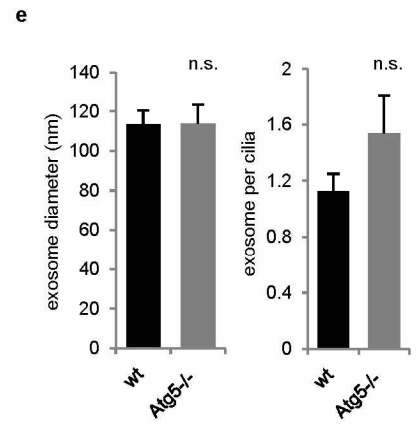
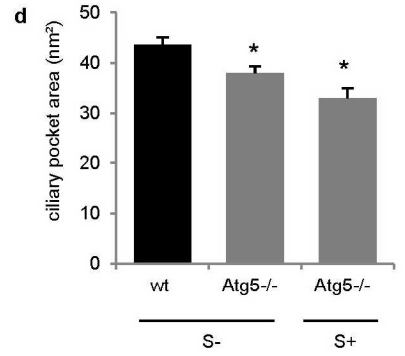
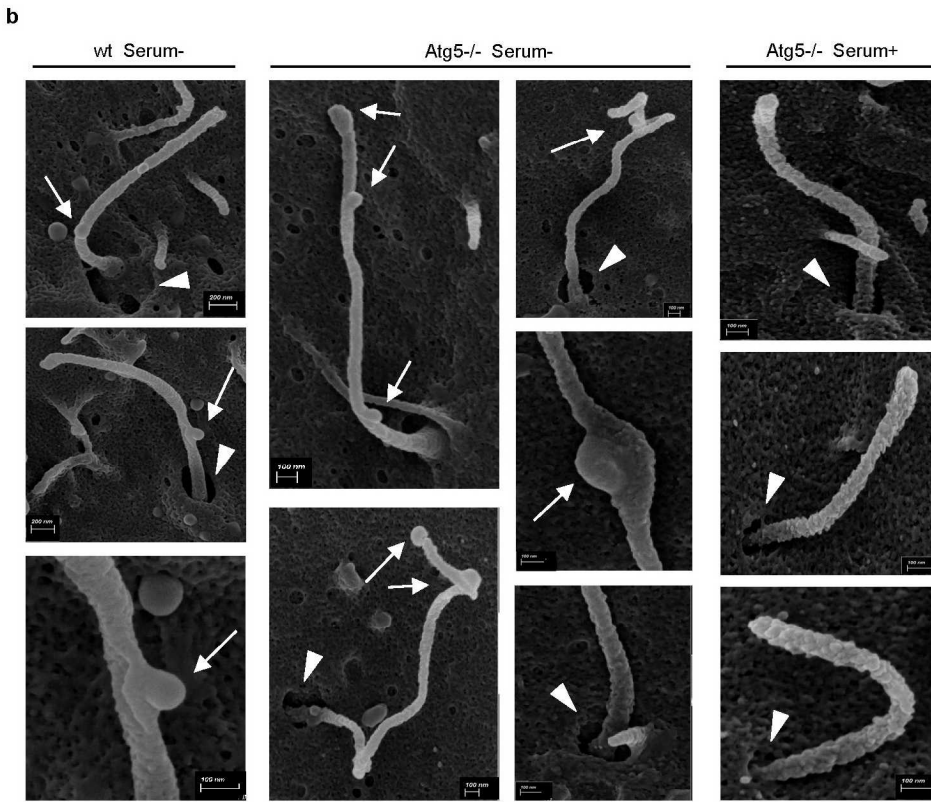
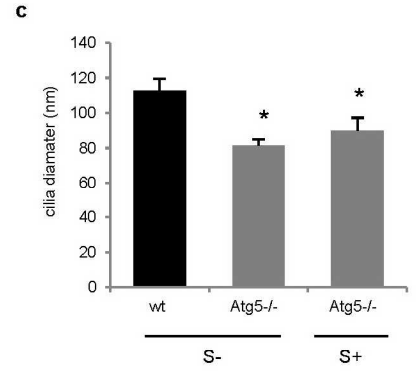
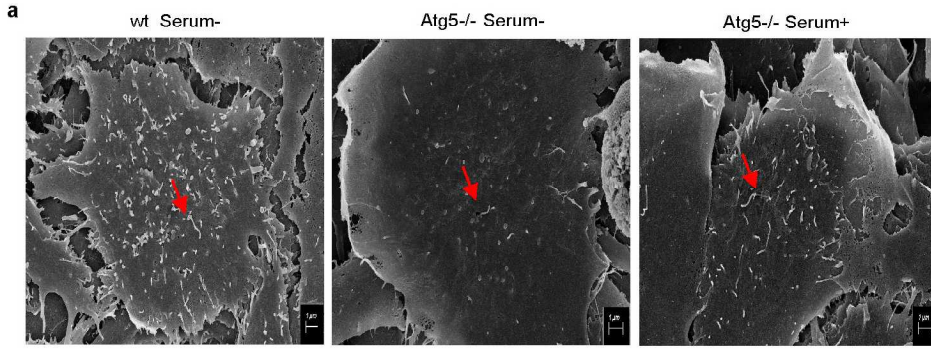
Filename: figure_2.jpg



Type of file: figure

Label: Extended Data Figure 10

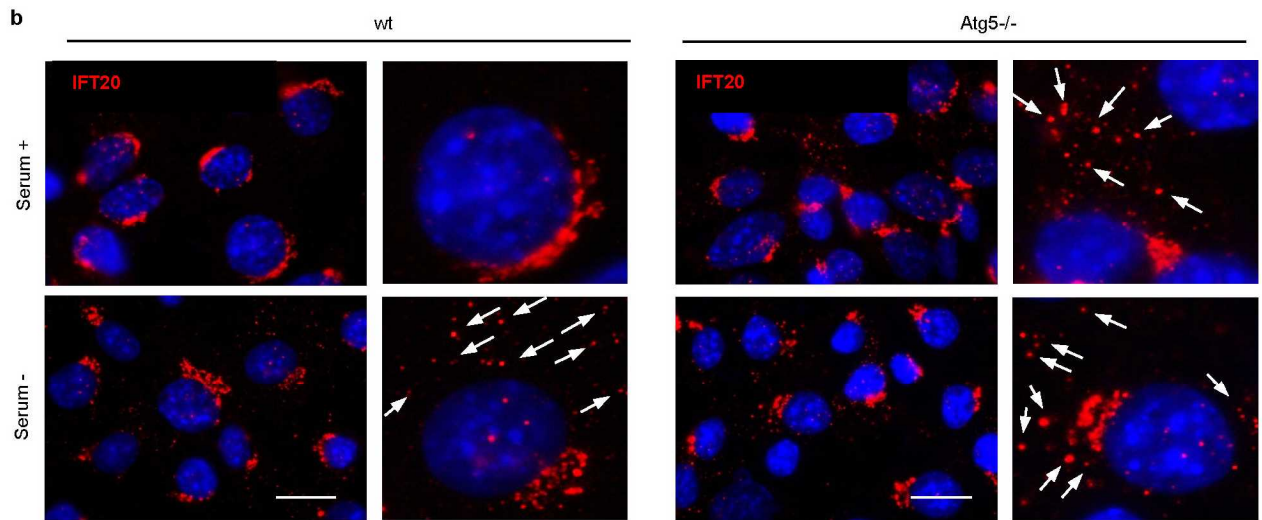
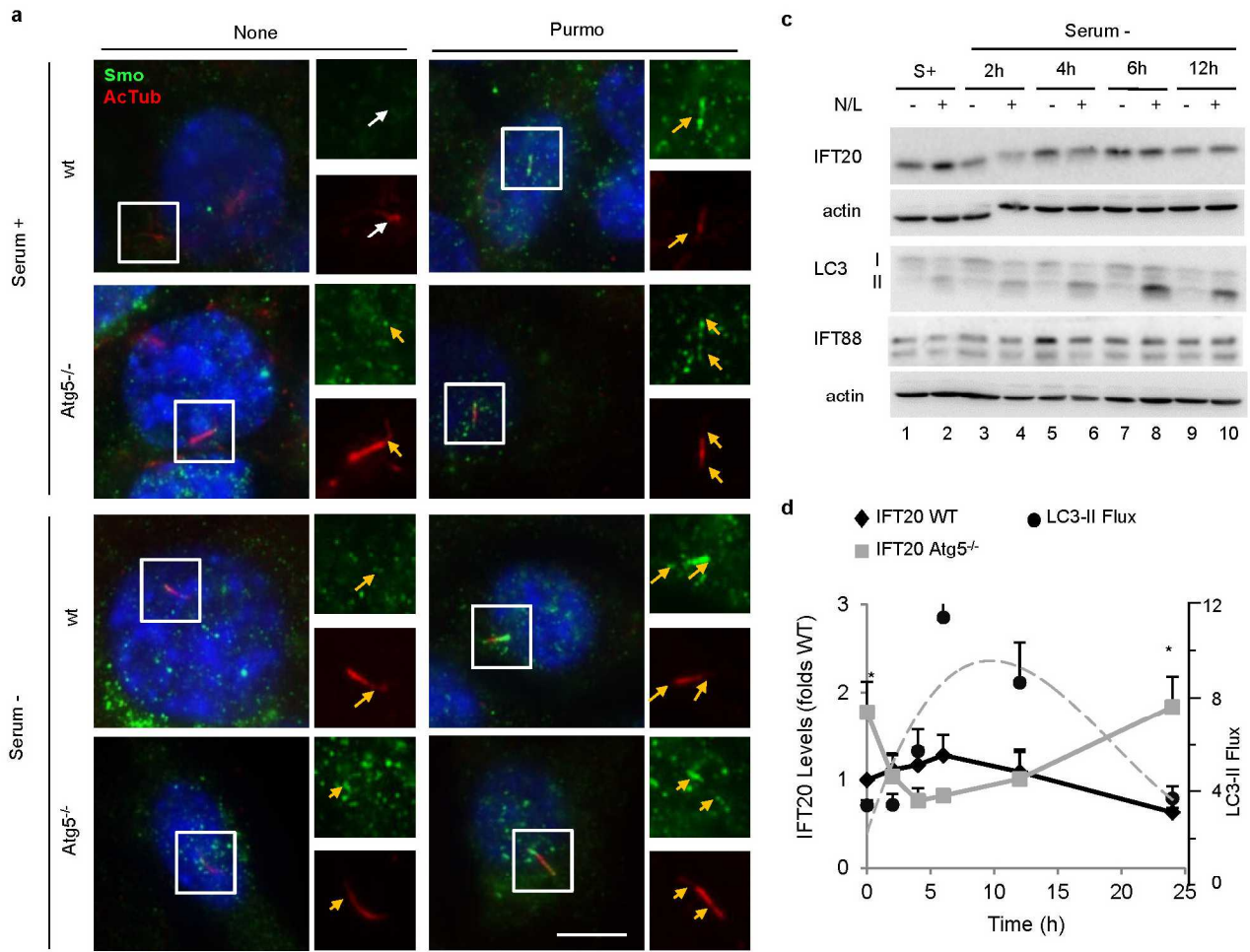
Filename: figure_11.jpg



Type of file: figure

Label: Extended Data Figure 11

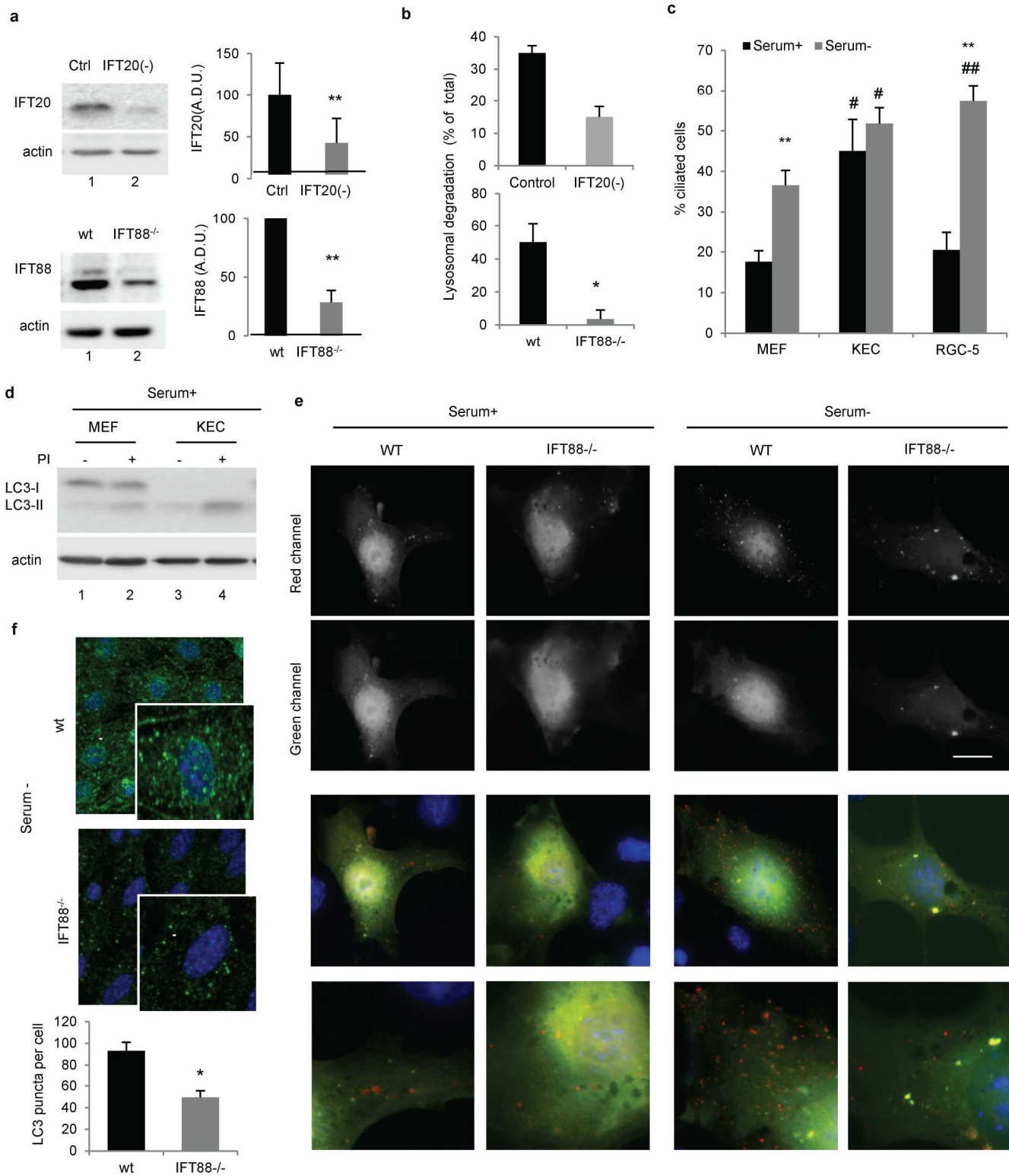
Filename: figure_12.jpg



Type of file: figure

Label: Extended Data Figure 2

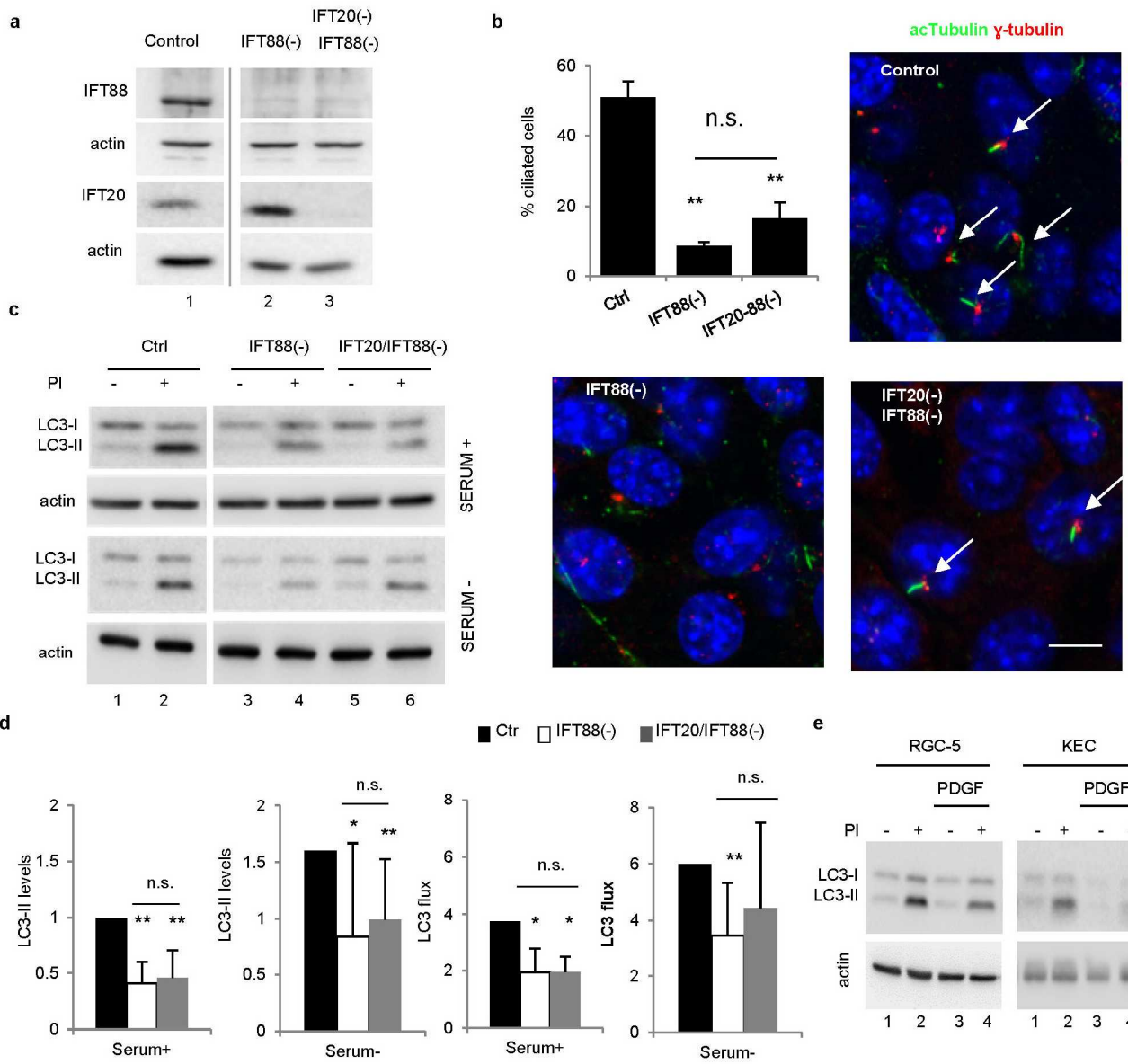
Filename: figure_3.jpg



Type of file: figure

Label: Extended Data Figure 3

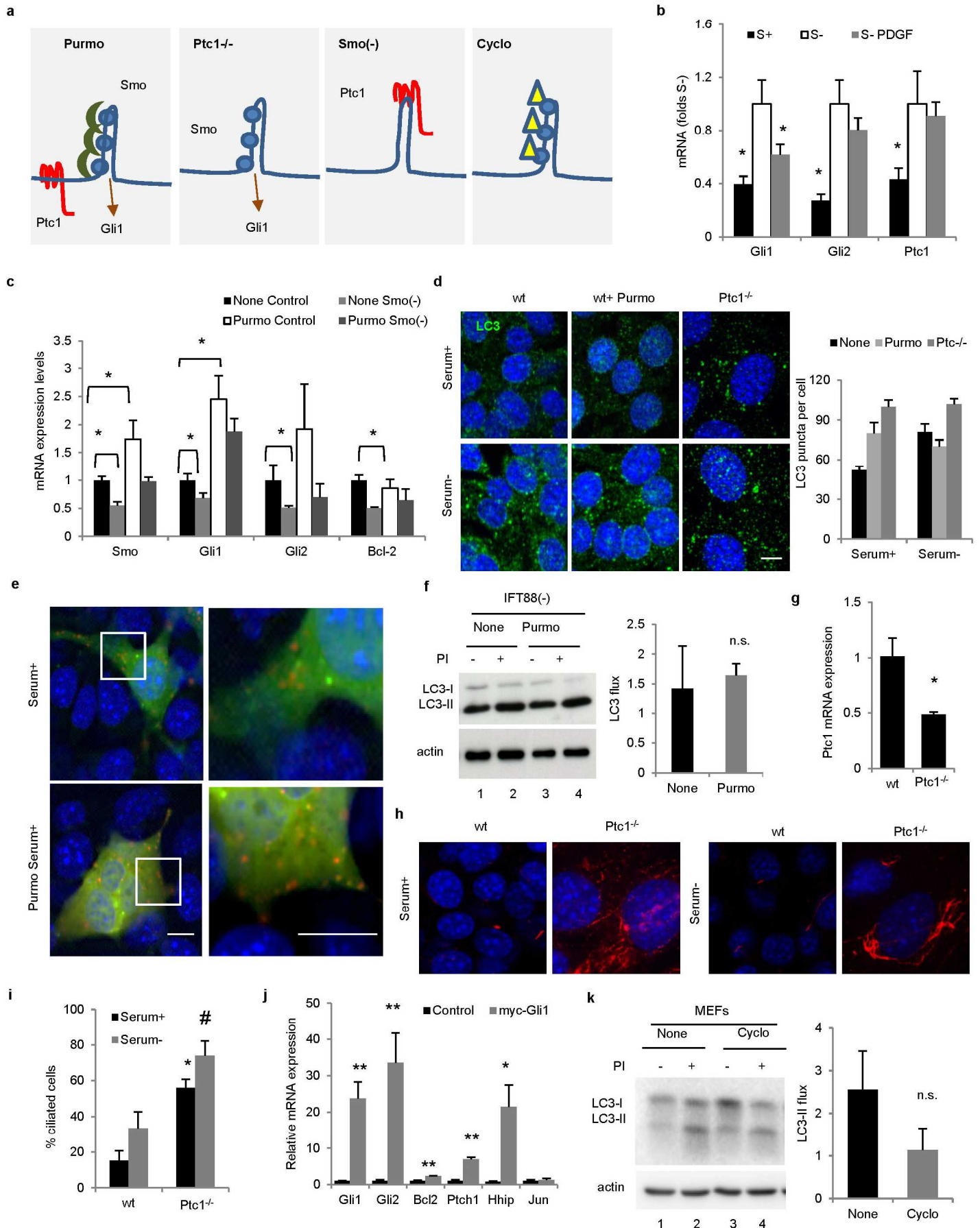
Filename: figure_4.jpg



Type of file: figure

Label: Extended Data Figure 4

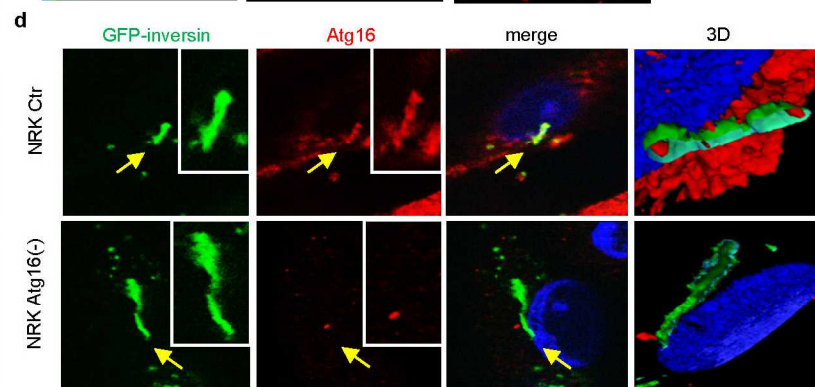
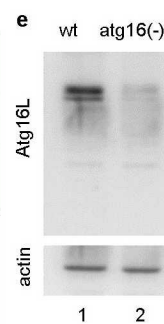
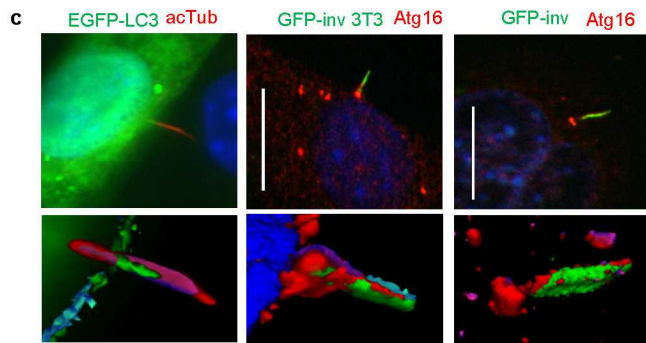
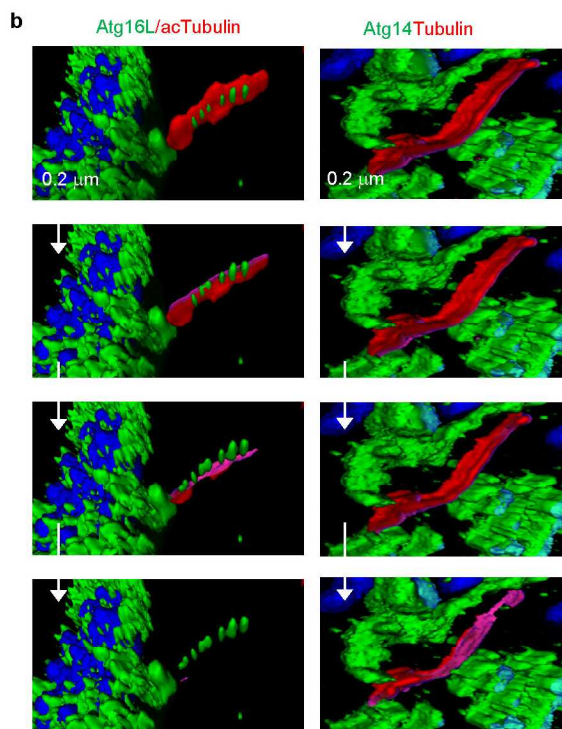
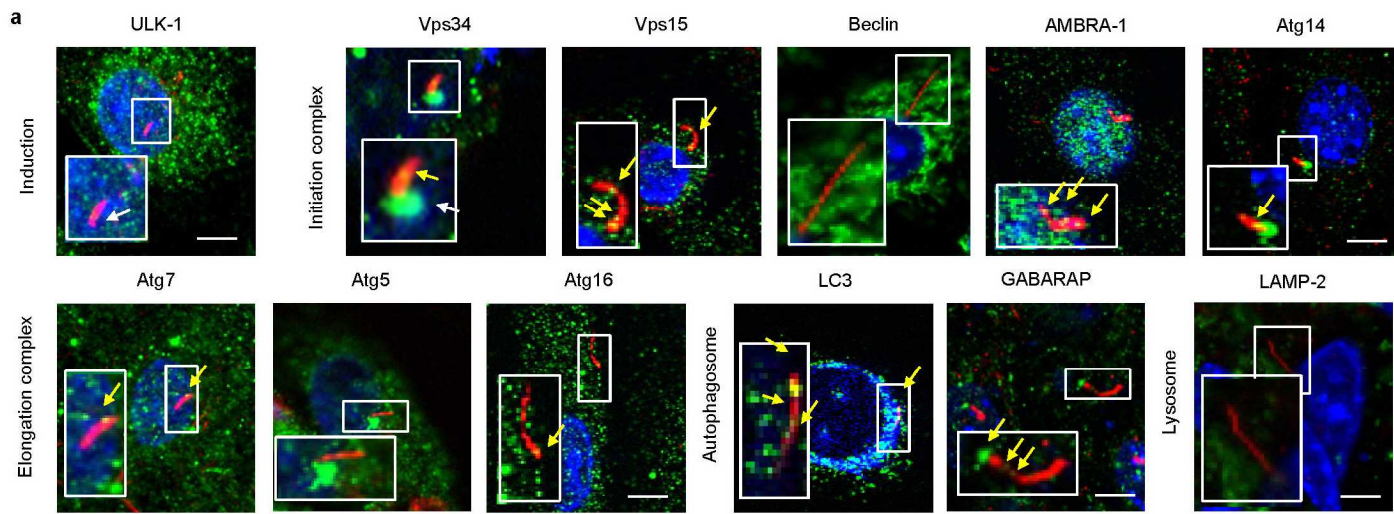
Filename: figure_5.jpg



Type of file: figure

Label: Extended Data Figure 5

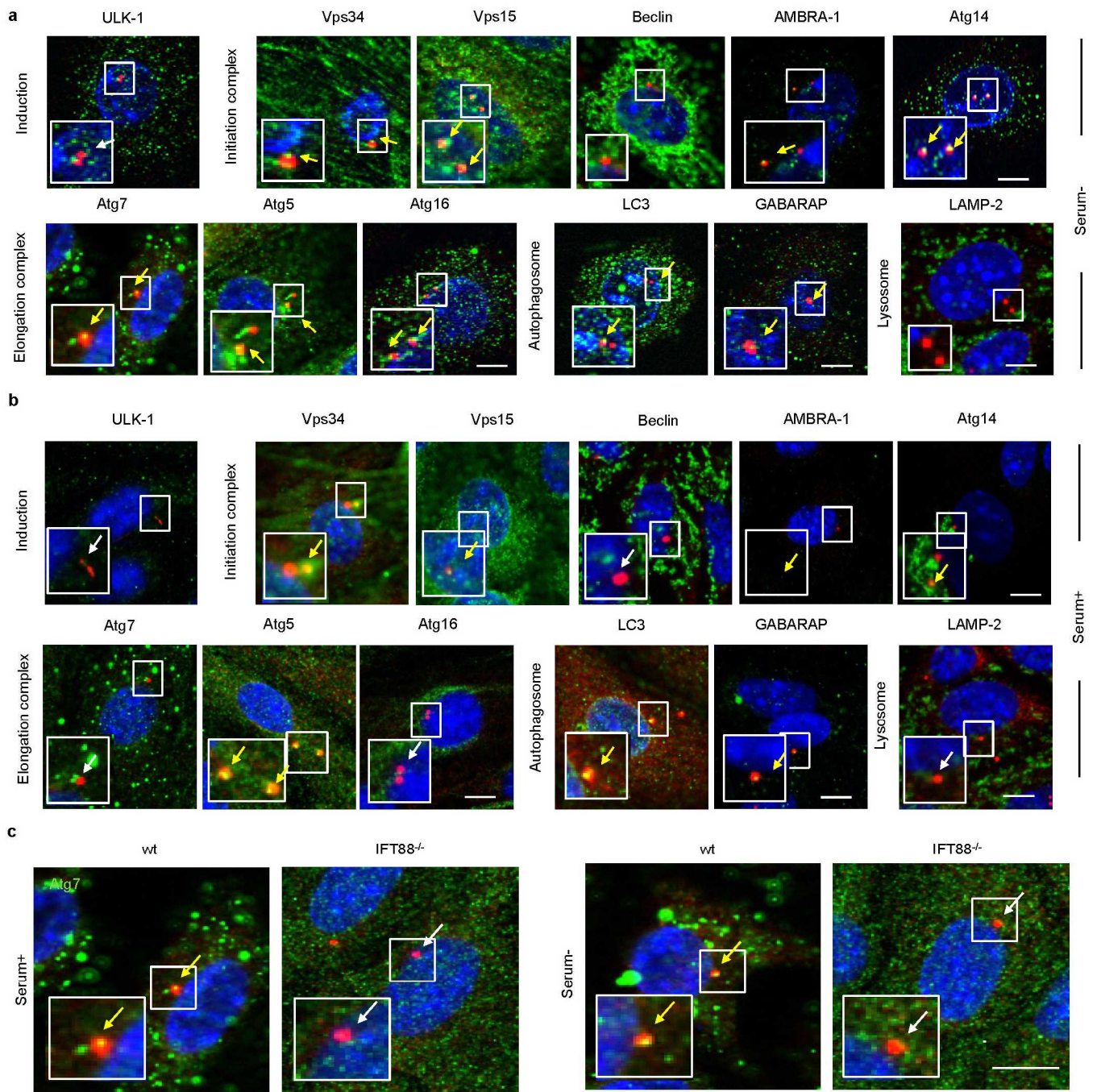
Filename: figure_6.jpg



Type of file: figure

Label: Extended Data Figure 6

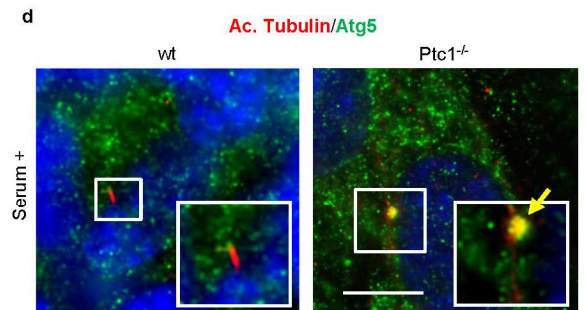
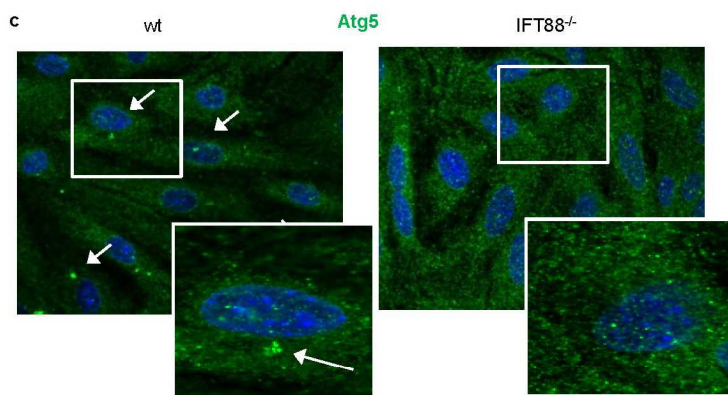
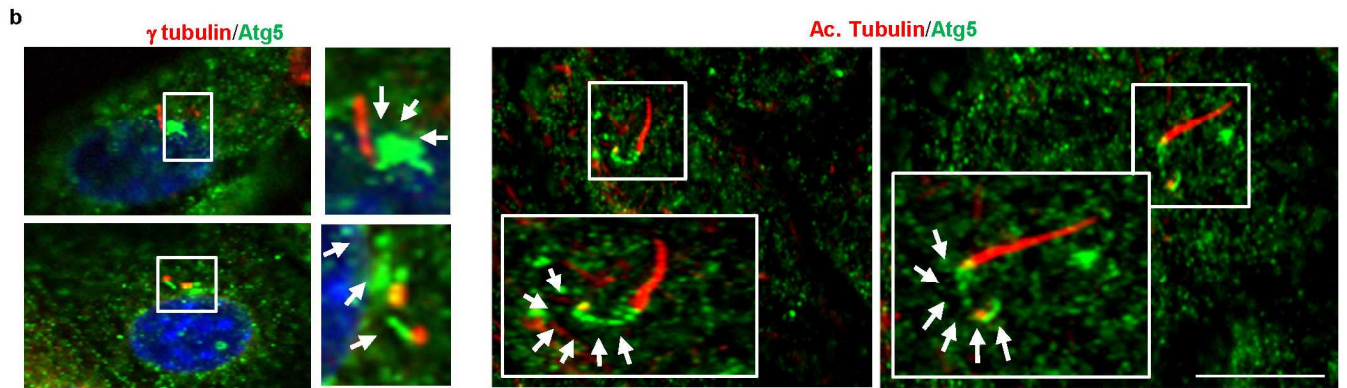
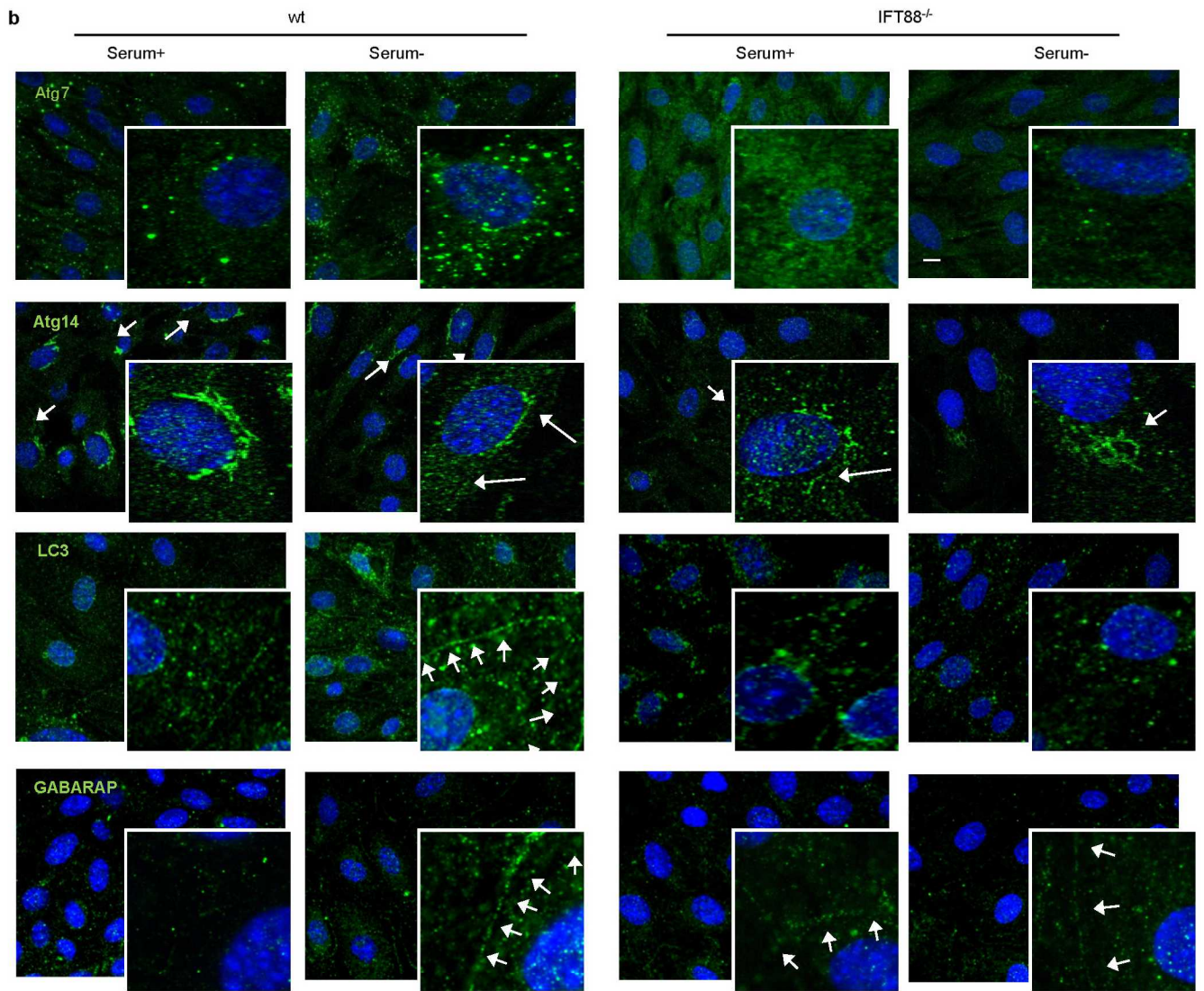
Filename: figure_7.jpg



Type of file: figure

Label: Extended Data Figure 7

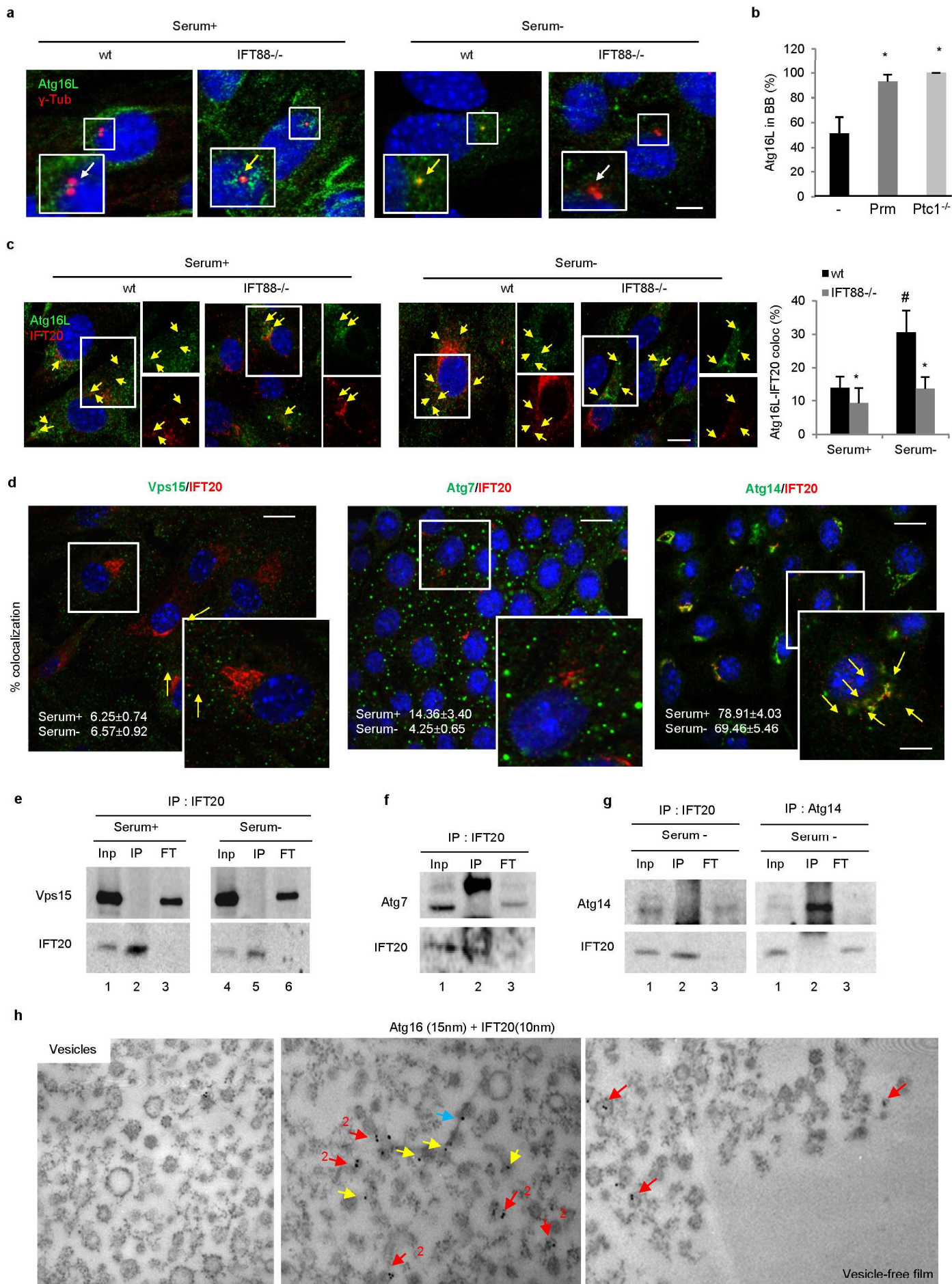
Filename: figure_8.jpg



Type of file: figure

Label: Extended Data Figure 8

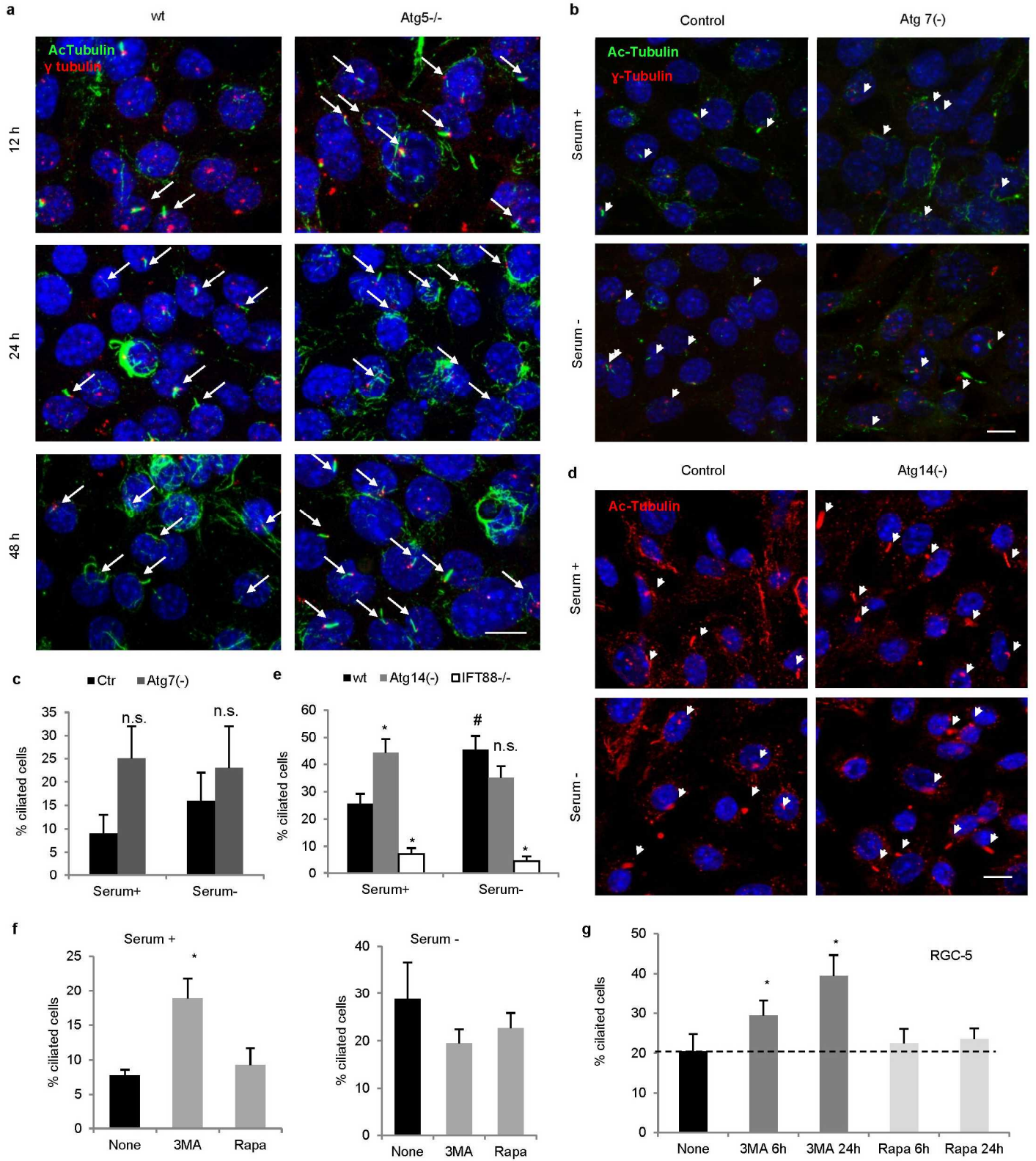
Filename: figure_9.jpg



Type of file: figure

Label: Extended Data Figure 9

Filename: figure_10.jpg



Type of file: figure

Label: Extended Data Figures 1 - 11

Filename: figure_13.pdf

